JOURNAL OF CATALYSIS 113, 398–409 (1988)

Carbon Monoxide Adsorption/Desorption Processes Over NaX Zeolite and Supported Ruthenium Catalyst

V. S. KAMBLE, N. M. GUPTA, AND R. M. IYER

Chemistry Division, Bhabha Atomic Research Centre, Bombay 400 085, India

Received October 1, 1987; revised January 13, 1988

The binding states of CO on NaX zeolite and RuNaX were investigated by thermal desorption spectroscopy. Desorption peaks centred at around 390, 430, 490, and 520 K were observed from NaX following room-temperature adsorption of CO. The activation energy values corresponding to these peaks were calculated to be 41.4, 45.7, 53.8, and 57.7 kJ mol^{-1}, respectively. These peaks were also observed in desorption profiles from RuNaX although their temperatures were higher by 10 to 20 K. In addition, the desorption spectra from RuNaX also comprised two high-temperature peaks at around 575 and 640 K. With both the RuNaX and the NaX samples, the temperature and relative intensities of the desorption peaks depended on pretreatment conditions and on the lapsed time between CO exposure to the sample and the commencement of programmed heating. Mass spectral analysis revealed that the gas desorbed at 300–500 K consisted mainly of CO while at higher temperatures CO_2 was the main component. The desorption peaks below 500 K are attributed to the release of carbon monoxide from structural and intragranular or intergranular zeolitic pores. Lewis sites on the zeolite surface are found to facilitate activation of CO, resulting in its transformation to CO_2. The initial adsorption of carbon monoxide in zeolite pores and subsequent diffusion to metal sites leading to its disproportionation/oxidation is found to play an important role in the CO adsorption/desorption process on RuNaX.

INTRODUCTION

Catalytic hydrogenation of CO is now believed to proceed via active surface carbon intermediates, formed in disproportionation of CO over metal surfaces (*1–4*). The product distribution in the process is found to be strongly dependent on the metal and support material. The metal–metal interactions in the case of multicomponent catalysts and the metal–support interactions in the supported catalysts have therefore been the subjects of many individual studies and several reviews (*4–6*). In addition to altering the electronic properties of deposited metal, the support plays an important role of providing higher metal dispersion, resulting in a larger contact area and a reduction in the sintering of metal particles. Zeolites find a special place as supports and transition metals supported on zeolites exhibit characteristic catalytic activity for cracking, isomerisation, and oxidation reactions of hydrocarbons (*6*). Bifunctional behaviour arises in these catalysts due to two types of site: metallic sites for hydrogenation/dehydrogenation and zeolite acid sites for cracking and isomerisation.

Zeolite-supported Group VIII metals have also been investigated for carbon monoxide methanation and the Fischer–Tropsch (F–T) process. The activity and selectivity to form different products are reported to be significantly affected by the nature of the zeolite used as support (*7–11*). The role of the zeolite support in these processes is, however, not yet well understood. For example, it is not clear whether carbon monoxide is also adsorbed on the zeolite support in addition to that on the metal surface. It if is then what are the adsorption sites and how does CO adsorbed on the zeolite contribute to the overall

0021-9517/88 $3.00

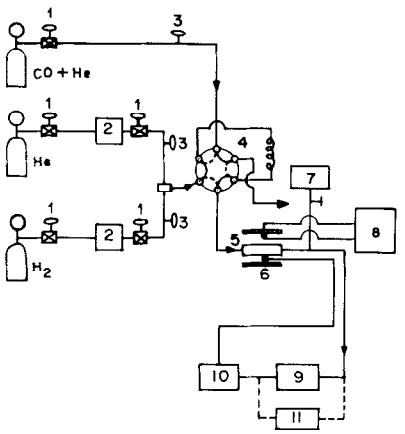

FIG. 1. Schematic diagram of thermal desorption spectroscopy unit: 1, flow control valve; 2, gas purification system; 3, shut-off valves; 4, gas sampling valve; 5, catalytic reactor; 6, furnace; 7, vacuum pump; 8, temperature programmer; 9, gas chromatograph; 10, recorder; 11, mass spectrometer.

hydrogenation process? Another important question is whether zeolites could activate CO molecules as in the case of hydrocarbons.

To answer some of these questions, the adsorption states of carbon monoxide on zeolite NaX and on RuNaX catalyst have been investigated in this study using temperature desorption spectroscopy (TDS). Mass spectrometry and gas chromatography were employed to analyse the thermally desorbed gases. Auger electron spectroscopy was used for surface analysis before and after using the samples for CO TDS. This study is a continuation of work reported earlier (*1*) on the nature and reactivity of transient species formed in the methanation of CO and CO_2 over Ru/zeolite-X catalysts.

EXPERIMENTAL

Temperature Desorption Spectroscopy

The schematics of the instrumentation used for TDS studies is shown in Fig. 1. The catalyst was housed in a stainless-steel tube reactor of 0.4 cm i.d. and could be heated under H_2, He, or vacuum in any sequence without in-between exposure to air. Carbon monoxide pulses were injected over the sample using a gas sampling valve system. Before a TDS profile was recorded, the sample was pretreated *in situ* by heating in succession in H_2 (625 K, 16 h, 50 ml min^{-1}), under vacuum (10^{-1} Torr, 875 K, 30 min), and then in helium (875) K, 1 h, 50 ml min^{-1}). The effect of pretreatment at lower temperatures was also evaluated. The sample at this stage was cooled to room temperature under helium flow and then about 10 carbon monoxide pulses (each containing 5.8 μmol CO mixed with 17 μmol of He) were introduced in succession to completely saturate the sample with CO. After the release of loosely held CO, the desorption spectra were recorded in the dynamic system using He as a carrier gas (50 ml min^{-1}) and a linear heating rate of 30 K min^{-1}. The effect of time lapsed between CO exposure and commencement of the heating programme was investigated by allowing the sample to equilibrate for 1 to 18 h at 298 K in helium flow following the last CO injection as mentioned above.

The effluent gases were analysed independently with a gas chromatograph using a thermal conductivity detector and a mass spectrometer (VG Micromass 7070 F) coupled with the catalytic reactor through stainless-steel tubes. While the thermal conductivity detector gave the total yield of evolved gases (say CO and CO_2), the mass spectral analysis enabled the determination of individual peak composition.

The activation energy values corresponding to different desorption peaks were evaluated using the expression

$$\frac{E_d}{2.303RT_m} = 2 \log T_m - \log \beta - \log \frac{E_d}{\nu R}, \quad (1)$$

where the terms E_d, T_m, β, ν refer to the activation energy of desorption, the temperature at the peak maximum, the heating rate, and the frequency factor, respectively (*12*). If the frequency factor may be pre-

sumed to be around 10^{13} s^{-1}, i.e., of the order of molecular vibratrional frequency, then the third term on the right-hand side of Eq. (1) may be considered negligible and the above expression reduces to

$$\frac{E_d}{2.303RT_m} = 2 \log T_m - \log \beta. \quad (2)$$

Activation energy values were also evaluated by measuring T_m for different β values and plotting $\ln(\beta/T_m^2)$ versus $1/T_m$. The values thus obtained for different peaks were 10–15 kJ mol^{-1} less than those calculated using Eq. (2). No considerations were, however, given to the possible effects of CO diffusion through zeolite pores in evaluating E_d values.

Materials

The 40- to 60-mesh fraction of sodium-X zeolite (from the Associated Cement Co. Ltd., India) used in these experiments had a Si:Al ratio of ~1.2 as evaluated by gravimetric analysis. The samples were washed repeatedly with demineralised water before use and then were dried for 10–15 h in a vacuum oven at 425 K.

Using the washed zeolites as support, the catalyst samples containing ~1.5 wt% of ruthenium were prepared using the incipient wetness method. The support material was wetted with the required amount of $RuCl_3$ (aqueous) solution, air-dried at 365 K while stirring, and reduced in flowing H_2 at 575 K.

Helium gas (99.9%) from Airco was used after processing through a bed of Deoxo catalyst and molecular sieve traps. A glass column containing dehydrated silica gel was connected to the molecular sieve traps to serve as an indicator for the possible presence of moisture in the helium carrier gas. No colour change in silica gel was detected even after using the purification system for several months. Hydrogen gas was used after purification with a Matheson Model 8262 purifier. Carbon monoxide from Airco was used without further purification.

Characterization

The fresh samples and also those used for TDS experiments were examined by powder X-ray diffraction (XRD) using a conventional diffractometer (Cu$K\alpha$ radiation).

The surface composition was analysed by Auger electron spectroscopy using a PHI Model 551 electron spectrometer employing a 3-keV electron beam. Pellets of 1 cm diameter and about 1–2 mm thickness were used for this purpose and were degassed for 6 h at 425 K in a vacuum oven and then for 24 h at 300 K in the spectrometer prechamber (~10^{-6} Torr). The charging shifts in the Auger peaks were calibrated with respect to the 510-eV KLL signal from oxygen.

The heat of carbon monoxide adsorption was evaluated by gas chromatography. For this purpose, the specific retention volume (V_g) was determined for differing catalyst bed temperatures (T_c) and the ΔH values were evaluated from the plots of $\ln(V_g/T_c)$ vs $1/T_c$ (*13*).

The zeolite acid strength was evaluated by titration with *n*-butylamine using bromothymol blue as an indicator. Prior to acid strength measurement, the sample was pretreated in N_2 gas flow for 6 h at 675 K.

The intragranular and intergranular pore size distributions in the zeolite (macropores) were evaluated by the mercury intrusion method using a Micromeritics Auto Pore Model 9200 porosimeter. The samples used for this purpose were prepared by pressing 1.5 g of material at 10,000 kg pressure.

RESULTS

1. Sample Characteristics

Table 1 gives the characteristics of NaX and RuNax catalyst samples used in this study. The X-ray diffraction pattern from these samples corresponded to the spectrum reported for NaX zeolite (*14*). Also, the repeated carbon monoxide adsorption/desorption cycles did not result in significant modification of XRD profiles confirm-

TABLE 1

Characteristics of NaX Zeolites and Ru (1.5%)/NaX Catalyst

Sample	N_2 adsorption surface area[a] ($m^2\ g^{-1}$)	Heat of CO adsorption[b] ($-\Delta H$) (kJ mol^{-1})	Acid strength[c] (mmol g^{-1})
NaX	332	14.9	0.46
Ru/NaX	300	14.5	—

[a] By BET method using N_2.
[b] By gas chromatography.
[c] Titre value for *n*-butylamine.

ing that no lattice distortions are produced during heating and cooling of samples under the present experimental conditions.

Figure 2 shows the typical macropore distribution present in the pelletised NaX samples as determined by mercury porosimetry. An almost similar pore size distribution was observed from RuNaX. The intragranular and intergranular pores would similarly exist in zeolite samples packed in our catalyst column, although the pore size distribution is likely to be different.

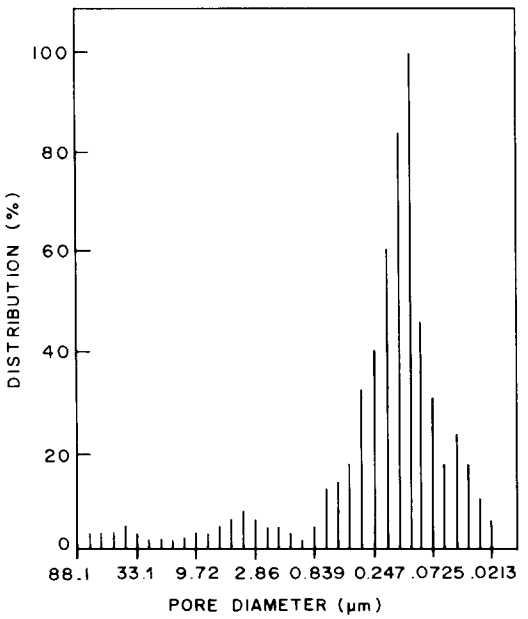

FIG. 2. Macropore distribution in NaX as evaluated by the mercury intrusion method.

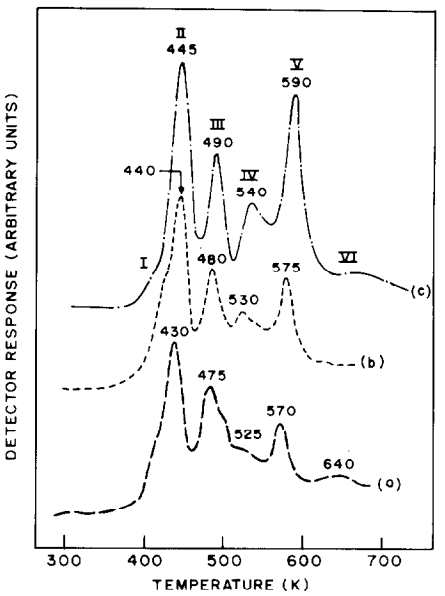

FIG. 3. Thermal desorption spectra obtained on exposure of CO over differing amounts of RuNaX. (a) 150 mg, (b) 300 mg, (c) 500 mg.

2. *Thermal Desorption Spectra from RuNaX*

(i) Effect of sample amount. To ascertain the readsorption effects in the catalyst bed, the desorption spectra were recorded using different quantities of catalyst. Figure 3 shows the carbon monoxide desorption spectra for three different sample amounts in the range 150–500 mg. At least six desorption peaks with maxima (T_m) at around 400, 440, 490, 530, 575, and 640 K, marked as peaks I–VI, respectively, could be discerned in these spectra. The activation energy values corresponding to these peaks as evaluated using Eq. (2) were 42.6, 47.5, 53.8, 64.7, and 73.2 kJ mol^{-1} respectively. As may be seen in Fig. 3, the general shape of the desorption spectra remained unaltered, although the T_m shifted to slightly higher values with increasing sample amount. A sample mass of 300 mg was considered to be optimum in terms of peak

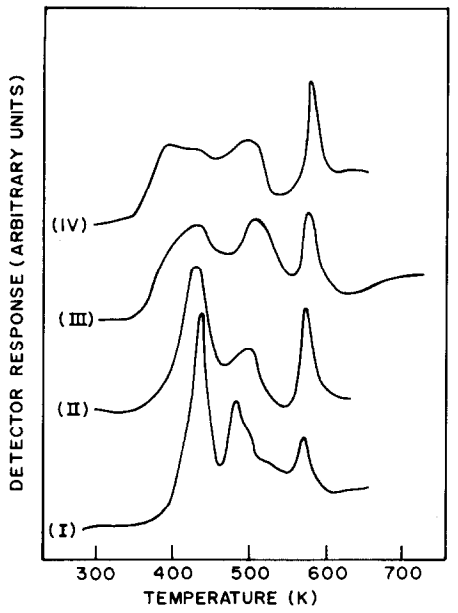

FIG. 4. TDS profiles from a 150-mg RuNaX sample during four consecutive CO adsorption–thermal desorption cycles.

resolution and was used for all the subsequent experiments reported in the text unless mentioned otherwise.

The time lapsed between carbon monoxide exposure to the sample and commencement of the heating programme had a considerable effect on the desorption spectra, as will be discussed shortly. The spectra in Fig. 3 were recorded with a 1-h time lapse.

(ii) Desorption spectra in consecutive CO adsorption/desorption cycles. Consecutive carbon monoxide adsorption/desorption cycles using the same sample resulted in progressive broadening of the first three peaks, as is shown in the data of Fig. 4 for RuNaX. In between two consecutive CO adsorption/desorption cycles when the sample was heated without introducing CO, no effluents were observed confirming that no residual gases remained adsorbed on the sample subsequent to a CO adsorption/desorption cycle. Also, the time delay between two consecutive adsorption/desorption cycles had no significant effect on the TDS data. For example, the spectra II and III of Fig. 4 were recorded with an in-between time interval of about 30 min while the interval between spectra I and II and that between III and IV was around 16–18 h during which the samples were maintained under He flow. This confirmed that no extraneous impurities are present in the system to affect the desorption profiles.

(iii) Effect of sample preparation and thermal pretreatment. It was desirable to evaluate the adsorption behaviour of different batches of independently prepared RuNaX samples. Spectra a and b of Fig. 5 show the TDS profile from 300 mg of RuNaX prepared in two different batches employing the same method as that for the sample used to obtain the data of Figs. 3 and 4. The CO TDS spectra from different RuNaX batches gave peaks with almost

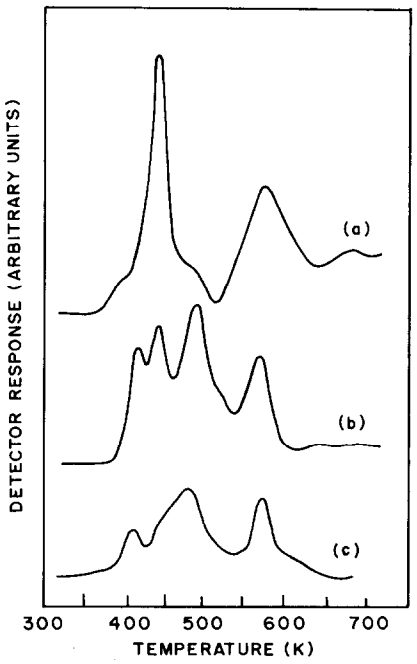

FIG. 5. Curves (a,b), TDS profiles from 300-mg RuNaX samples from different batches both pretreated in H_2 (625 K, 16 h), under vacuum (875 K, 30 min), and in He (875 K, 1 h) followed by room-temperature exposure to CO. Curve (c), same sample as that used for curve (b) but pretreated in H_2 (625 K, 16 h), under vacuum (625 K, 30 min), and in He (625 K, 1 h) before CO exposure.

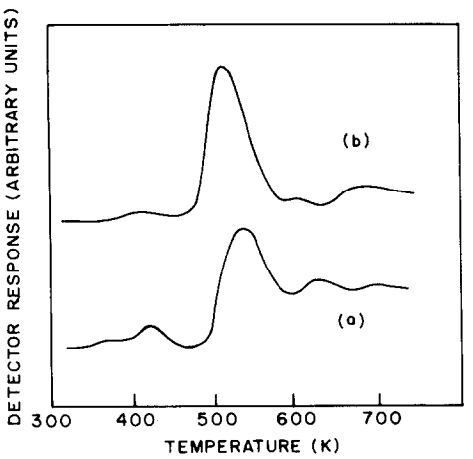

FIG. 6. TDS profiles from RuNaX obtained for (a) 8-h and (b) 16-h time intervals between CO exposure and commencement of heating cycle.

similar T_m although their relative intensities were considerably different.

The thermal treatment of the sample prior to CO adsorption also had a significant effect on the desorption profile. Instead the sample being heated at 875 K under vacuum and then in helium as indicated earlier, a sample was pretreated similarly at lower temperatures (<650 K) prior to room-temperature CO adsorption; the desorption peaks were then less intense and their relative intensities were modified. A typical desorption profile from a sample similar to that for Fig. 5b but pretreated at 625 K is shown in Fig. 5c.

(iv) Effect of time delay between CO injection and heating cycle. With an increasing time lapse between the last CO injection and heating commencement, the intensity of peaks I–IV decreased progressively while that of peak V increased. Figure 6 shows the TDS profiles recorded for time intervals of 8 and 16 h.

(v) Desorbed gas composition. Figure 7 shows the mass spectral analysis of the effluent gases released in a typical desorption cycle. The effluent desorbed up to a sample temperature of about 500 K consisted of only CO while at higher temperatures either CO_2 alone or CO_2 mixed with a small amount of CO was observed. Although the yields of CO and CO_2 were not very reproducible, the nature of the TDS profile was always found to be similar in consecutive CO adsorption/desorption cycles. In cases when the time interval between the last CO pulse injection and heating cycle was large, e.g., 16 h, the desorbed gas (i.e., Fig. 6b) consisted of mainly CO_2.

3. Thermal Desorption Spectra from NaX

Figures 8a–8c show the effect of thermal pretreatment on the TDS profile from 300 mg of NaX sample recorded 1 h after being exposed to 10 CO pulses as described earlier. The profile consists of peaks with maxima at around 390, 430, 490, and 520 K. The activation energy values associated with these peaks were calculated to be 41.4, 45.7, 53.8, and 57.7 kJ mol^{-1}, respectively. With an increase in sample pretreatment temperature the peaks at $T_m < 500$ K decreased in intensity while the high-temperature peak (520 K) grew larger, as is shown in Fig. 8.

The effect of consecutive adsorption/desorption cycles and that of CO injection–heating time gap on temperature desorption spectra from NaX were similar to those from RuNaX samples. For example, spectrum d in Fig. 8 shows the TDS profile recorded with a 16-h CO injection–heating cycle gap. It may be observed in Fig. 8d that with an increased lapse of time the

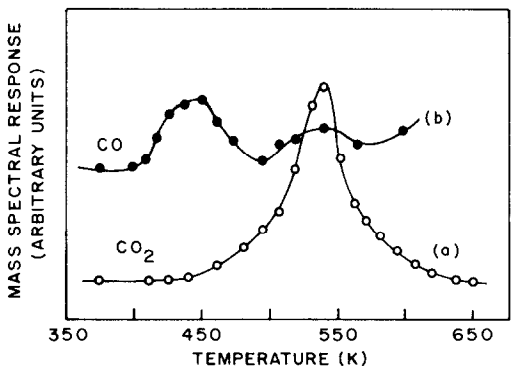

FIG. 7. CO and CO_2 desorption profiles from RuNaX following room-temperature CO adsorption.

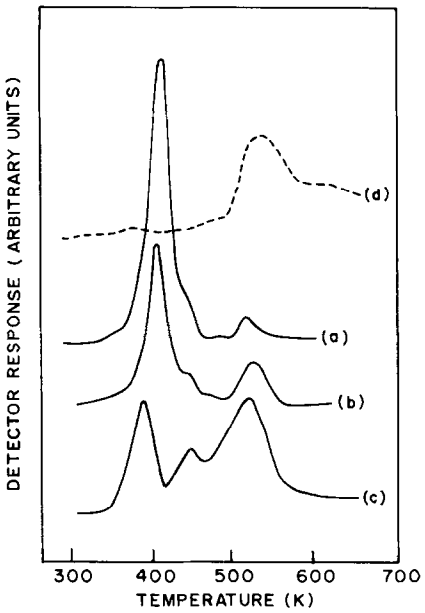

FIG. 8. TDS profiles from NaX following CO adsorption, curves (a–c) were recorded under the following pretreatment conditions: curve (a) H_2 (600 K, 6 h), vacuum (600 K, 30 min), He (600 K, 1 h); curve (b) H_2 (600 K, 6 h), vacuum (675 K, 30 min), He (675 K, 1 h); curve (c) H_2 (600 K, 16 h), vacuum (875 K, 30 min), He (875 K, 1 h). Curve (d) shows TDS profile for the CO adsorption–heating interval of 18 h, the interval in the case of curves (a–c) being 1 h.

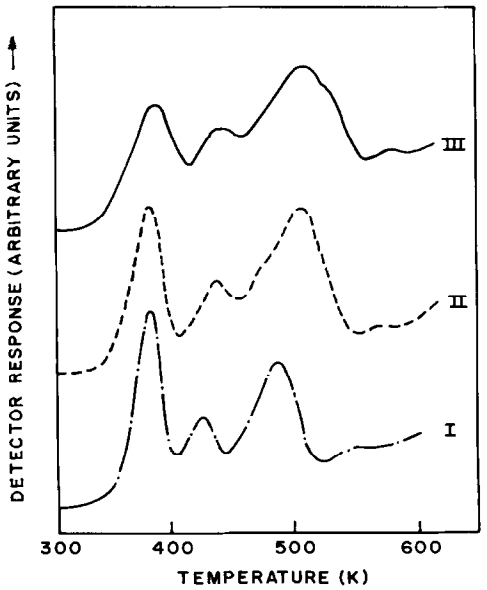

FIG. 9. TDS profiles from a NaX sample during consecutive CO adsorption/desorption cycles.

low-temperature peaks became smaller while the intensity of the 520 K peak increased.

Figure 9 shows three consecutive CO adsorption/desorption profiles from a 300-mg NaX sample. While the time lapsed between the recordings of spectra I and II was 17 h, spectrum III was recorded soon after the second adsorption/desorption cycle.

Mass spectral analysis of the desorbed gas stream is shown in Fig. 10. It may be observed that, as in the case of RuNaX, the peaks at T_m less than 500 K consisted basically of CO while those at higher temperature were predominantly due to CO_2. Also, when the CO injection–heating cycle gap was 16 h, the desorbed gas corresponding to Fig. 8d was mainly CO_2.

4. Desorption from Blank Sample

The following experiment was carried out to confirm that the carrier helium did not contain any contaminants (e.g., H_2O, O_2, or CO_2), which after becoming adsorbed with time in the zeolite bed could affect the TDS data. A 300-mg NaX sample was treated successively in H_2, under vacuum, and in He as described under Experi-

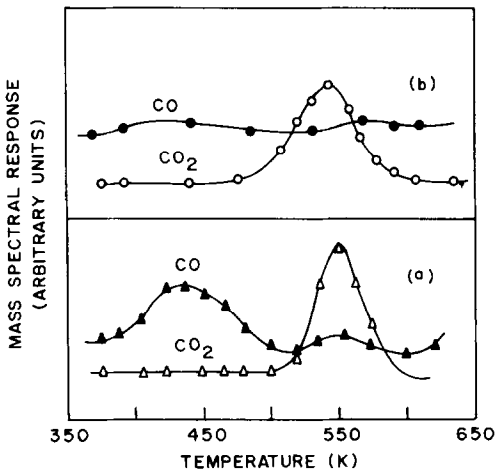

FIG. 10. CO and CO_2 desorption profiles from NaX following CO adsorption, CO adsorption–heating commencement gap for curve (a) 1 hr and for curve (b) 16 hr.

TABLE 2

Effect of Thermal Treatment prior to Room-Temperature CO Exposure over NaX and RuNaX and That of the Time Interval between CO Exposure and Heating Commencement on the Amounts of CO and CO_2 Released during Programmed Heating

Sample	Pretreatment temperature (K)	CO exposure–heating cycle gap (h)	Amount of desorbed gas (μmol)		Desorption spectrum (figure no.)
			CO ±10%	CO_2 ±10%	
RuNaX	875	1	1.30	0.25	4b
	875	1	1.41	0.27	6a
	875	8	0.16	1.09	7a
	875	16	0.05	1.10	7b
	625	1	0.77	0.14	6b
NaX	875	1	0.67	0.54	9c
	875	16	0.01	0.63	9d
	675	1	0.89	0.19	9b
	600	1	1.15	0.04	9a

mental and was then cooled to room temperature. A TDS profile recorded at this stage showed only a slight baseline shift. The sample was then maintained under He flow at 297 K for 18 h and when a desorption spectrum was recorded again, no TDS pattern or baseline shift was observed.

5. *Comparative CO and CO_2 Yields*

Comparative yields of CO and CO_2 desorbed as a function of pretreatment temperature and the carbon monoxide injection–heating commencement gap are given in Table 2. These data represent the integrated area under different peaks considering the desorption peaks below 500 K to be due to CO and those at higher temperatures to be due to CO_2. It may be noted that in two batches of RuNaX samples, although desorption peaks had varying relative intensities, the overall amounts of CO and CO_2 evolved were almost the same. Similar results were obtained with other batches of RuNaX samples. If we compare corresponding data from NaX and RuNaX (Table 2), we find that the total amount of desorbed CO + CO_2 and particularly that of CO_2 are higher from RuNaX. With an increasing time gap between CO exposure and heating commencement the yield of desorbed CO_2 increased considerably, while that of CO decreased in the cases of both RuNaX and NaX samples.

6. *Auger Analysis*

Auger spectra of both the NaX and the RuNaX samples after usage for the CO adsorption/desorption process showed the presence of a prominent KLL carbon peak at 272 eV. In the Auger spectra from NaX and RuNaX, which were not exposed to CO, the intensity of the carbon peak was negligibly small. Argon ion sputtering for 8–10 min was able to remove carbon from CO-exposed samples, thus confirming its presence only at the surface.

DISCUSSION

Binding states of CO over transition metals have been widely investigated using clean metal surfaces (*15*) as well as supported catalysts (*16–22*) wherein different forms of CO–metal bonding have been advocated. Most of the studies on supported metals have used alumina or silica as supports and offer varying views regarding

carbon monoxide adsorption states. Foger and Anderson (*16*), for example, observed that thermally desorbed gases from Pt/Al_2O_3 and Pt/Aerosil subsequent to room-temperature CO adsorption contained CO_2 in addition to CO and the formation of CO_2 was attributed to a catalysed reaction between CO and traces of residual H_2O. Zagli *et al.* (*18*) similarly reported the thermal desorption of CO and CO_2 from the surface of supported Ni catalysts following CO adsorption. Multiple CO desorption chromatograms have been reported by Choi *et al.* (*19*) in their carbon monoxide TDS study on Co/Al_2O_3 catalysts and these have been attributed to different metal sites. It has also been suggested that the alumina support is activated at temperatures above 575 K and its oxygen reacted with CO to produce CO_2. Rieck and Bell (*21*) have shown that in Pd/La_2O_3 a portion of lanthana in close contact with Pd particles undergoes reduction to form LaO_x moieties. The LaO_x moieties also facilitate the dissociation of CO, a key step in carbon monoxide methanation. In the study by Lee *et al.* (*17*) on Ni/SiO_2 it was observed that C and O remained on the catalyst surface subsequent to CO adsorption followed by thermal desorption of CO and CO_2. The desorption peaks were attributed to carbon monoxide bonded in linear and bridged forms at metal sites. Galuszka *et al.* (*23*) reported that temperature-programmed desorption of CO from Ni/Al_2O_3 occurs in a single peak before 575 K. Some of the CO was found to be disproportionated and carbon thus formed reacted with lattice oxygen to again form CO.

The role of the support, particularly that of molecular sieves, in CO adsorption/desorption over supported catalysts has, however, not yet been investigated in detail.

The results of the present study may be summarized as follows.

(I) At least four distinct CO adsorption sites exist over NaX giving rise to desorption peaks at 390, 430, 490, and 520 K. The desorption spectra from RuNaX comprised two additional high-temperature peaks at ~575 and 640 K in addition to the peaks observed from NaX (although at slightly higher T_m).

(II) The gases desorbed from both NaX and RuNaX at temperatures lower than 500 K consist mainly of CO while CO_2 is the main component at higher temperatures. The amount of desorbed CO + CO_2 is higher from RuNaX than that from NaX (Table 2).

(III) The thermal pretreatment of the sample prior to room-temperature CO adsorption has a considerable effect on the relative peak intensities (Figs. 5 and 8), the effect being more pronounced in the case of NaX. The higher the pretreatment temperature, the greater is the intensity of the 520 K peak, i.e., the amount of desorbed CO_2 (Table 2).

(IV) The desorption spectra recorded with different time gaps between CO exposure to the sample and the heating commencement (Figs. 6 and 8) show that CO and CO_2 are retained for a considerable duration over both NaX and RuNaX under continuous gas flow conditions and CO diffuses with time to those sites where it becomes converted to CO_2 (Table 2).

(V) Auger spectroscopy results show that CO adsorption and subsequent thermal desorption result in surface carbon deposition on both the NaX and the RuNaX samples.

The carbon monoxide adsorption sites on our samples may be divided into two categories, (a) where CO is held and is thermally desorbed without accompanying chemical change and (b) where it is activated and converts to CO_2. The CO adsorbed in zeolites may be located either in cages or at surface sites. The structure formed on joining the sodalite cages in NaX has two types of pores or cavities in it: supercages (α-cages, diameter 1.3 nm, aperture 0.8 nm) and sodalite cavities (β-cages, diameter 0.66 nm, aperture 0.22

nm). However, with van der Waals diameter of 0.31 nm (*24*) the CO molecules may not enter the sodalite cages. In addition to the intracrystalline pore structure (micropores), the zeolite crystallites are bound together into granules giving rise to a second type of pore distribution (macropores). The typical macropore distribution in our sample is shown in Fig. 2. The CO adsorbed in different pore systems is expected to be thermally released without accompanying chemical transformation. The data obtained for repeated CO adsorption/desorption cycles (Fig. 4) show that the pore system entrapping the CO is modified in the process. XRD results, on the other hand, suggest that crystal structure and hence the zeolitic pore structure is not affected during CO adsorption/desorption cycles. It is therefore apparent that the modification in macropore distribution due to thermal sintering contributes significantly to the desorption profiles observed in our study. Although the present data do not allow the assignment of desorption peaks to the specific pores, it may be inferred that the peaks with T_m in the range 300–500 K are due to CO released from structural and intergranular zeolitic pores. The activation energy values for these desorption peaks are similar to those required for diffusion of simple molecules through zeolite pores (*25*).

In RuNaX samples, the ruthenium metal will be dispersed at the zeolite surface as well as in different pores. Complete or partial blocking of the pores by Ru crystallites would therefore result in the absence of certain desorption peaks or an increase in activation energy required for release of entrapped CO. This is in agreement with the data obtained from RuNaX (Figs. 3 and 5).

The desorption peaks in the range 500–650 K from RuNaX (Fig. 3) and at 520 K in NaX (Fig. 8) arise due to release of CO_2. Disproportionation of CO over Group VIII metals is a well-known phenomenon. The data of Table 2 show that the carbon monoxide initially adsorbed in zeolite pores diffuses with time to Ru sites, resulting in CO_2 formation. The multiple CO_2 peaks from RuNaX may be ascribed to disproportionation of CO at ruthenium located at different sites although our data do not completely rule out the possibility of part of the CO combining with lattice oxygen.

The formation of CO_2 on NaX (Fig. 10) is an interesting observation. Auger analysis (*26*) confirmed that no transition metal impurities were present in our samples. CO reaction with adsorbed water or zeolitic hydroxyl groups could be one possible source of CO_2 formation. However, the consistent CO_2 peak (~500 K) observed in TDS profiles in consecutive CO adsorption/desorption cycles (Fig. 9) indicates that formation of CO_2 by the CO oxidation route may not play a very important role. It is well known that the chemisorption of CO on Group VIII metals involves an acceptor–donor bond with electron transfer from the 5σ orbital of CO into the unoccupied metal orbitals and back-donation of metallic *d*-electrons into the antibonding $2\pi^*$ orbitals of CO (*4*). Lewis acid sites being the sites of surface unsaturation would similarly be expected to accept an electron pair from CO to form a chemisorption bond. The structure of some Lewis acid sites which could participate in CO chemisorption are shown in Scheme I (27). The open circle in these structures represents an electron hole. Figure 8 shows that on increasing the pretreatment temperature prior to room-temperature CO adsorption, the yield of CO_2 released on thermal desorption was considerably higher. It is well known that with a rise in temperature, particularly at more than 600 K, the hydroxyl group content of the zeolite decreases, resulting in the conversion of Brønsted sites to Lewis acid sites (*28*). The catalytic activity of different zeolites has been found to have a correlation with Lewis acidity. Barthomeuf (*28*), for example, has shown that the activity of acid-catalysed *n*-hexane cracking over NH_4Y zeolite increased with pretreat-

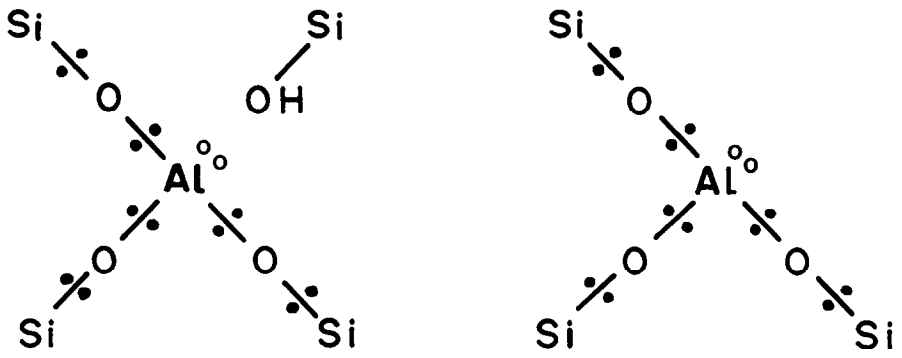

SCHEME 1

ment temperature in the range 600–850 K, which corresponded with a decrease in hydroxyl group content. A Lewis site assisted CO activation and dissociation over alumina-supported catalysts has recently been proposed by Odebunmi *et al.* (*29*). Our data can be interpreted to suggest that the zeolitic Lewis sites facilitate the chemisorption, activation, and dissociation of carbon monoxide molecules. The Auger analysis results have confirmed that the exposure of NaX to carbon monoxide and subsequent heating to 700 K results in the deposition of surface carbon, suggesting that the disproportionation of CO according to the Boudouard reaction is a possible step leading to CO_2 formation. Although an unequivocal description of the adsorbed CO configuration may not be possible at this stage, the studies on cation-exchanged zeolites (*26*) tend to support the Blyholder mechanism, i.e., with carbon directed towards the Lewis site.

CONCLUSIONS

1. Carbon monoxide is strongly adsorbed in different pores and at Lewis acid sites when exposed over NaX zeolite at room temperature and atmospheric pressure. At least four distinct CO adsorption sites are found to be present. In the case of RuNaX, the CO is held over different metal sites in addition to the zeolite pores.

2. Carbon monoxide adsorbed over Lewis acid sites and over ruthenium is converted to CO_2 on programmed heating.

3. The CO desorbed from zeolite pores on thermal activation either is released as such into the He carrier gas or diffuses to metal sites leading to CO_2 formation.

ACKNOWLEDGMENTS

The authors thank Shri K. Annaji Rao for help in mass spectral analysis and Dr. R. Bhat for evaluation of pore size distribution by mercury porosimetry.

REFERENCES

1. Gupta, N. M., Kamble, V. S., Annaji Rao, K., and Iyer, R. M., *J. Catal.* **60,** 57 (1979).
2. Ponec, V., *Catal. Rev. Sci. Eng.* **18,** 151 (1978).
3. Bell, A. T., *Catal. Rev. Sci. Eng.* **23,** 203 (1981).
4. Vannice, M. A., *in* "Catalysis Science and Technology" (J. R. Anderson and M. Boudart, Eds.), Vol. 3, p. 139. Springer-Verlag, Berlin, 1982.
5. See papers in "Metal Support and Metal Additive Effects in Catalysis" (B. Imelik *et al.*, Eds.). Elsevier, Amsterdam, 1982.
6. Gates, B. C., Katzer, J. R., and Schuit, G. C. A., "Chemistry of Catalytic Processes." McGraw–Hill, New York, 1979.
7. Elliott, D. J., and Lunsford, J. H., *J. Catal.* **57,** 11 (1979).
8. Chen, Y. W., Wang, H. T., and Goodwin, J. G., Jr., *J. Catal.* **83,** 415 (1983); **85,** 499 (1984).
9. Leith, I. R., *J. Catal.* **91,** 283 (1985).
10. Jacobs, P. A., *in* "Catalysis by Zeolites" (B. Imelik *et al.*, Eds.), p. 293. Elsevier, Amsterdam, 1980.
11. Ballivet-Thatchenko, D., Coudurier, G., and Mozzanega, H., *in* "Catalysis by Zeolites" (B. Imelik *et al.*, Eds.), p. 309. Elsevier, Amsterdam, 1980.
12. Cvetanovic, R. J., and Amenomiya, Y., "Advances in Catalysis" (D. D. Eley, P. W. Selwood, and P. B. Weisz, Eds.), Vol. 17, p. 103. Academic Press, San Diego, 1967.
13. Atkinson, D., and Curthoys, G., *J. Chem. Ed.* **55,** 564 (1978).

14. Barrer, R. M., Baynham, J. W., Bultitude, F. W., and Meier, W. M., *J. Chem. Soc. (London)*, 195 (1959).
15. Morris, M. A., Bowker, M., and King, D. A., *in* "Comprehensive Chemical Kinetics" (C. H. Bamford, C. F. H. Tipper, and R. G. Compton, Eds.), Vol. 19, p. 1. Elsevier, Amsterdam, 1984.
16. Foger, K., and Anderson, J. R., *Appl. Surf. Sci.* **2,** 335 (1979).
17. Lee, P. I., Schwarz, J. A., and Heydweiller, J. C., *Chem. Eng. Sci.* **40,** 509 (1985).
18. Zagli, A. E., Falconer, J. L., and Kennan, C. A., *J. Catal.* **56,** 453 (1979).
19. Choi, J. G., Rhee, H. K., and Moon, S. H., *Appl. Catal.* **13,** 269 (1985).
20. Agnol, C. D., Gervasini, A., Morazzoni, F., Pinna, F., Strukul, G., and Zanderighi, L., *J. Catal.* **96,** 106 (1985).
21. Rieck, J. S., and Bell, A. T., *J. Catal.* **85,** 143 (1984); **96,** 88 (1985); **99,** 278, 262 (1986).
22. Erdöhelyi, A., and Solymosi, F., *J. Catal.* **84,** 446 (1983).
23. Galuszka, J., Chang, J. R., and Amenomiya, Y., *J. Catal.* **68,** 172 (1981).
24. "C. R. C. Handbook of Chemistry and Physics" (R. C. Weast, Ed.), p. F-211. CRC Press, Boca Raton, FL, 1979.
25. Ruthven, D. M., Loughlin, K. F., and Derrah, R. I., *Adv. Chem. Ser.* **121,** 330 (1973).
26. Kamble, V. S., Gupta, N. M., and Iyer, R. M., in press.
27. Anderson, J. R., *in* "Structure of Metallic Catalysts," p. 69. Academic Press, San Diego/London, 1975.
28. Barthomeuf, D., *in* "Zeolites: Science and Technology" (F. R. Ribeiro *et al.*, Eds.), NATO ASI Ser. E., No. 80, p. 317. 1984.
29. Odebunmi, E. O., Zhao, Y., Knözinger, H., Tesche, B., Manogue, W. H., Gates, B. C., and Hulse, J., *J. Catal.* **86,** 95 (1984).